Colour modulation of blue anthocyanin-derivatives. Lignosulfonates as a tool to improve the water solubility of natural blue dyes.

Paula Araújo[§1], Nuno Basílio[§2], Joana Azevedo[1], Ana Fernandes[1], Nuno Mateus[1], Fernando Pina[2], Victor de Freitas[1], Joana Oliveira[1*]

[1] ICETA/REQUIMTE – Laboratório Associado para a Química Verde, Departamento de Química e Bioquímica, Faculdade de Ciências, Universidade do Porto, Rua do Campo Alegre, 687, 4169-007 Porto, Portugal,

[2] REQUIMTE – Laboratório Associado para a Química Verde, Departamento de Química, Faculdade de Ciências e Tecnologia, Universidade Nova de Lisboa, 2829-516 Monte de Caparica, Portugal.

Author to whom correspondence should be addressed, [*]jsoliveira@fc.up.pt

Tel: +351.220402596

[§] These authors contributed equally to the paper.

ICETA/REQUIMTE

REQUIMTE

ABSTRACT

The impact of a lignosulfonate (calcium) (**L**) on the chromatic features of two anthocyanin-derived bluish dyes (portisin, **P** and pyranoanthocyanin dimer, **PD**) was evaluated in aqueous solutions using UV-Visible spectroscopy. It was demonstrated that the interaction between each dye and this macromolecule at pH 1 occurs by two mechanisms, association and copigmentation that are dependent on **L** concentration. For

instances, at low concentrations of **L** (up to 0.27 µM) it is observed the association of dyes promoted by their complexation with lignin (different molecules of dye are bound to the same binding sites of **L**). At higher concentrations of **L** (25 µM), the aggregation of dyes decreases and each molecule is bound to a different site of **L** resulting in the formation of a charge-transfer complex (copigmentation). Moreover, the titration of both dyes (**P** and **PD**) in the presence of **L** (19 µM) showed a strong stabilization of their pyranoflavylium cation forms revealed by the considerably higher pK_{a1} (6.6±0.1 and 6.2±0.1 for **P** and **PD**, respectively) in the presence of this macromolecule when compared to the values obtained in the absence (pK_{a1}= 4.61±0.03 and 4.93±0.04).

In addition, the water solubility of the dyes in the absence and presence of **L** was also evaluated by turbidimetry and the results showed that the water soluble lignosulfonate improved the solubility of the dyes over time.

Keywords: portisins; pyranoanthocyanin dimers; calcium lignosulfonate; colour; aggregation; charge-transfer complex.

1. Introduction

Colour is the first quality parameter perceived in many products such as foodstuffs and beverages, makeups, cloths and others. Therefore, colorants (natural or synthetic) play a crucial role for the valorisation of the final product. Blue dyes are rare in nature, thereby constituting a challenging research field. Nevertheless, the only function of synthetic colorants is to confer colour to things. On the other hand, natural colorings present significant benefits comparatively to the synthetic ones, since many of them present antioxidant, anti-inflammatory and other biologic properties.

Over the last years, our research group has done important work on the isolation and hemi-synthesis of anthocyanin-derived pigments found in red wines during ageing [1, 2]. This includes the identification of different families of anthocyanin-derived pigments that present unusual bluish colours at acidic pH [1], namely, the detection and identification in aged Port wines of a family of pyranoanthocyanin-dimers displaying a turquoise-blue colour [2]. Studies performed in model solutions showed that these compounds are formed from the reaction between methylpyranoanthocyanins and carboxypyranoanthocyanins. Although these molecules present attractive blue colors at low pH, their industrial application as dyes is limited due to their poorly hydrosoluble nature.

Lignin represent an average 25% of the terrestrial plant biomass being the second most abundant natural substance after cellulose [3]. Depending on the extraction method, it is possible to obtain different types of lignins, namely alkali, hydrolytic, kraft, organosolv and sulphite (lignosulfonates). The different lignin types could have various industrial applications such as energy, chemicals, dispersants, sorbent, surfactant, carbon fibers, plastics and more yet to come [3-6].

Lignosulfonates are water soluble compounds produced from softwood in the sulfite pulping method during the manufacturing of paper. In this process, bisulfite ions react with the native lignin polymer of the wood to form sulfonated lignin increasing the water-solubility of the hydrophobic lignin polymer [7]. Lignosulfonates have been used for a number of years in the food industry, serving, for example, as an emulsifier in animal feed, as raw material in the production of vanillin, and as a boiler water additive. Moreover, personal care and cosmetic formulations containing lignosulfonates have also been described [8, 9].

Bearing this, the goal of this work was to study the interaction of a lignosulfonate (calcium) (**L**) with two anthocyanin-derived bluish dyes (portisins, **P** and pyranoanthocyanin dimer, **PD**) (**Figure 1**), the impact on their colour features and its ability to improve the water solubility of these dyes using UV-Visible spectroscopy and turbidimetry, respectively.

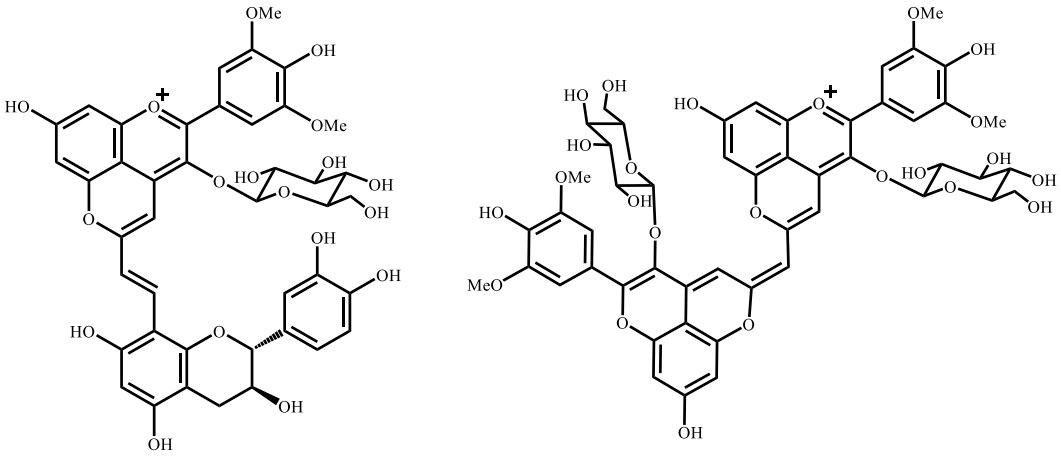

Figure 1 – Structure of the Portisin (**P**) and Pyranomalvidin-3-glucoside (**PD**) dyes in their pyranoflavylium cation form.

2. Material and Methods

2.1. Reagents.

A universal buffer (1 L) of Theorell and Stenhagen [10] was prepared dissolving 2.25 mL of phosphoric acid 85% (w/w), 7.00 g of monohydrated citric acid, 3.54 g of boric acid and 343 mL of a 1 M NaOH solution. Calcium Lignosulfonate (Molecular Weight 40.000 – 65.000 $g.mol^{-1}$) (**L**) United States Pharmacopeia (USP) Reference Standard was obtained from LGC Standards.

2.2. Hemi-synthesis and purification of blue dyes.

A-type portisin (**P**) and pyranomalvidin-3-glucoside dimer (**PD**) were obtained from the reaction of the A-type vitisin with (+)-catechin (in the presence of acetaldehyde) and methylpyranomalvidin-3-*O*-glucoside, respectively. The obtained dyes were purified by semi-preparative HPLC and structurally characterized as reported elsewhere [2, 11].

2.3. Determination of dye-lignin association constants.

The dye-lignin association constant was determined for **P** and **PD** at pH 1 by UV-Visible spectroscopy. For that, each dye was prepared in a solution of 0.1 M HCl at a concentration of 44 μM (Solution A). Similarly, a solution containing the dye at the same concentration and **L** at a concentration of 58 μM was prepared (Solution B). Solutions containing different concentrations of **L** (from 0.029 to 25 μM) were obtained by adding different volumes of the Solution B to the Solution A. For the determination of the molar concentrations of **L** an average molecular weight of 52.000 $g.mol^{-1}$ was used. The UV-Visible spectrum of all solutions were recorded in a 10x10 mm quartz cuvette in a Varian-Cary 100 Bio spectrophotometer from 350 to 800 nm.

The fittings for dye-lignin association constants determination were carried out using the Solver program from Microsoft Excel.

2.4. pH titration of dyes in the presence of lignin by UV-Visible spectroscopy.

The pH titration of dyes **P** and **PD** were performed in the presence of **L** by direct pH jump between 2.0 and 11.5. Stock solutions of dyes **P** and **PD** (180 μM) and **L** (77 μM) were prepared in 0.1 M HCl. 250 μL of a 0.1 M NaOH solution was added to a 10 mm pathlength plastic cuvette, 250 μL of Theorell and Stenhagen universal buffer solution at different pH values from pH 2.0 and 11.5, 25 μL of a 1 M NaOH solution, 250 μL of the **L** stock solution (final concentration of 19 μM) and 250 μL of the dye stock solution (final concentration was 44 μM). Spectra from 350 to 750 nm were recorded instantly after the addition of the dye (pseudo-equilibrium) and after one day (equilibrium) in a Varian-Cary 100 Bio spectrophotometer at 25ºC. The pH values of all solutions were measured in a Radiometer Copenhagen PHM240 pH/ion meter. The pH meter was calibrated with pH 4 and 7 buffer solutions. The fittings for pKa's determination were carried out using the Solver program from Microsoft Excel.

2.5. Impact of lignin on solubility and stability of the dyes.

The impact of **L** on the solubility of the dyes **P** and **PD** was determined by turbidimetry in a HACH 2100 N (ISO method 7020) turbidimeter calibrated with a StablCal® calibration set (< 0.1 – 1000 NTU). Solutions of each dye with different concentrations (20, 40, 80 and 160 μM) were prepared in a pH 3.5 citrate buffer (10 mM). Similar solutions were prepared containing 1 g/L (20 μM) of **L**. The turbidity of the solutions was measured immediately, after 1 and 30 days of storage at room temperature in the dark. The stability of the dyes in the presence of **L** during storage (0, 1, 3, 6 and 30 days) in the dark at room temperature was evaluated by UV-Visible spectroscopy in a Thermo Scientific Evolution Array UV-Visible spectrophotometer (360 – 830 nm) at 25ºC.

3. Results and discussion

3.1. Interaction between portisins (P) or pyranoanthocyanin dimer (PD) and lignin (L).

To evaluate the interaction of a lignin derivative (calcium lignosulfonate) (**L**) with A-type portisins (**P**) and pyranoanthocyanin dimers (**PD**) dyes, the dyes-lignin association constants were determined at pH 1 using UV-Visible spectroscopy. For that, the spectra of solutions containing the dye at a constant concentration (44 μM) and different concentrations of **L** (from 0.029 to 58 μM) were recorded between 350 and 800 nm.

Figure 2 shows the results obtained for the interaction of **P** with different concentrations of **L** and the inset shows the spectrum of the dye in the absence and in the presence of a low (0.27 μM) and a high concentration of **L** (25 μM) at pH 1. The spectral variations clearly show the existence of at least two interactions processes. At lower concentrations the band centred at 546 nm decreases in intensity and undergoes a very small bathochromic shift (~2 nm). These changes occur with a concomitant increase of a "shoulder" around 650 nm. The presence of an isosbestic point can also be detected at 584 nm. These spectral features show strong resemblance to those observed for anthocyanin aggregation phenomena [12]. Together with the well-known ability of polyelectrolytes to induce aggregation in oppositely charged dyes, the observed spectral changes suggest that **L** induce the aggregation of **P** at low macromolecule concentrations (below 0.28 μM) [13-18].

As the concentration of **L** increases it is possible to observe an important bathochromic displacement (~40 nm) on the maximum absorption wavelength (λ_{max}) of **P**. Conversely, to the spectral features observed at low **L** concentration, these results show similar features to copigmentation phenomena [19]. Similar results were observed for the interaction of **PD** with **L**, as seen in **SI** – **Figure 1**.

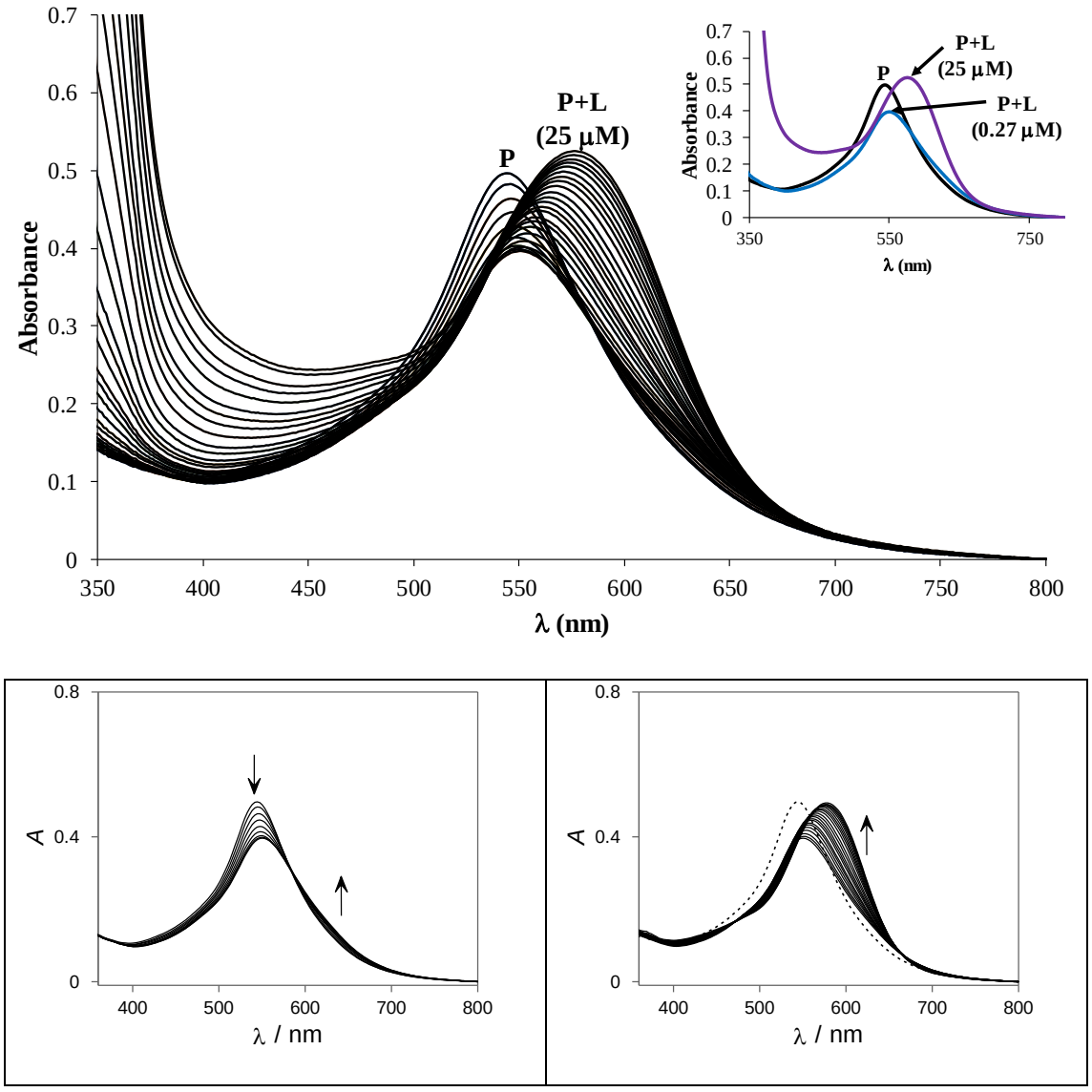

Figure 2 – Visible spectra of **P** with different concentrations of **L** and the inset shows the spectrum of the pigment in the absence and in the presence of a low (0.27 µM) and a high (25 µM) concentration of **L** at pH 1. Visible spectra of **P** (10 µM) at pH = 1 with different concentrations of **L:** from 0 to 0.27 µM (left) and from 0.27 µM to 25 µM (right). The spectrum of **P** in the absence of **L** is also shown for comparison (dotted line). All spectra were corrected by subtracting the corresponding absorption of **L**.

The graphical representation of the absorbance at 546 and 600 nm as a function of the concentration of **L** of the solutions with a fixed concentration of **P** is presented in **Figure 3**. A close inspection of these figures allows to evidence the existence of three distinct

processes (four populations of dye with different spectral features). In order to provide a semi-quantitative analysis of these results a model is proposed based on the "single set of identical sites" model [20, 21] where each binding site corresponds to a domain in the macromolecule (**L**) that can bind up to three **P** molecules. If a macromolecule (**L**) with *n* binding sites is considered, concentration of sites ([S]) is given by [**S**] = n[**L**] and the fraction of occupied sites (θ_b) by the sum of sites occupied with 1, 2 or 3 dye molecules (**PL**, **P$_2$L** or **P$_3$L**, respectively):

$$\theta_b = \frac{[PL] + [P_2L] + [P_3L]}{[S]_t} = \frac{[PL] + [P_2L] + [P_3L]}{n[L]_t} \qquad (1)$$

Following this reasoning, the fraction of free sites is:

$$\theta_f = 1 - \theta_b = 1 - \frac{[PL] + [P_2L] + [P_3L]}{n[L]_t} \qquad (2)$$

and the mass balance for the dye is:

$$[P]_t = [P]_f + [PL] + 2[P_2L] + 3[P_3L] \qquad (3)$$

Now, the apparent binding constants for the complexation of dye molecules at the macromolecule binding sites can be defined:

$$K_{11} = \frac{\theta_{11}}{\theta_f [P]_f} => \theta_{11} = K_{11}\theta_f [P]_f \qquad (4)$$

$$K_{12} = \frac{\theta_{12}}{\theta_{11} [P]_f} => \theta_{12} = K_{11}K_{12}\theta_f [P]_f{}^2 \qquad (5)$$

$$K_{13} = \frac{\theta_{13}}{\theta_{12}[P]_f} => \theta_{13} = K_{11}K_{12}K_{13}\theta_f[P]_f{}^3 \qquad (6)$$

Combining the above equations, and after some algebraic operations, equation 7 can be deduced and (numerically) solved for any combinations of n, K_1, K_2, K_3 and total concentrations of macromolecule/dye to give the equilibrium concentration of $([P]_f)$ which is combined with the above equation to obtain the concentrations of the different complexes.

$$[P]_f{}^4 + \left(3n[L]_t - [P]_t + \frac{1}{K_{13}}\right)[P]_f{}^3 + \left(\frac{2n[L]_t - [P]_t}{K_{13}} + \frac{1}{K_{12}K_{13}}\right)[P]_f{}^2$$

$$+ \left(\frac{n[L]_t - [P]_t}{K_{12}K_{13}} + \frac{1}{K_{11}K_{12}K_{13}}\right)[P]_f - \frac{[P]_t}{K_{11}K_{12}K_{13}} = 0 \qquad (7)$$

Because the absorption at a given wavelength is given by absorption of all species:

$$A_{obs} = \varepsilon_{Lf}[P]_f + \varepsilon_{11}[PL] + 2\varepsilon_{21}[P_2L] + 3\varepsilon_{31}[P_3L] \qquad (8)$$

Equation 8 was fitted to experimental data to give the following parameters: n = 14, K_1 = 3.7x10^5 M^{-1}, K_2 = 2.1x10^6 M^{-1}, K_3 = 6.8x10^5 M^{-1} (**Figure 3A** and **Table 1**). This set of apparent/macroscopic binding constants does not provide information on the mechanism and nature of interaction between dye and the macromolecule but only a quantitative measurement on the partition of the different complexes between the different states and of their mole fraction distribution (**Figure 3B**). However, comparing the mole fraction distribution with the spectral variations observed for **P** as a function of the concentration of **L** it is possible to suggest that while for complexes **P$_3$L** it seems that dye-dye interaction is stablished by complexation induced aggregation, this seems to not be case

for **P_2L** where the spectral features are more compatible with a copigmentation process. A similar behaviour was observed for the interaction between **PD** with **L** (**SI - Figure 2**) and this is reflected in the similarity obtained for the association constants (K_a/M^{-1}) of both dyes in the presence of **L** (**Table 1**).

The two mechanisms of interaction between each dye (**P** or **PD**) and **L** are schematically represented in **Figure 3**. For low concentrations of **L** (up to 0.27 µM) (**Figure 4A**) it is observed the aggregation of dyes promoted by the lignin complexation where different molecules of dye bind to the same binding site of **L**. When the concentration of **L** increases up to 25 µM, the aggregation of dyes decreases and the number of dye molecule bonded to each site of **L** decrease (**Figure 4B**). As the λ_{max} increases importantly (~40 nm) this could indicate the formation of a charge-transfer complex resulting from a copigmentation event.

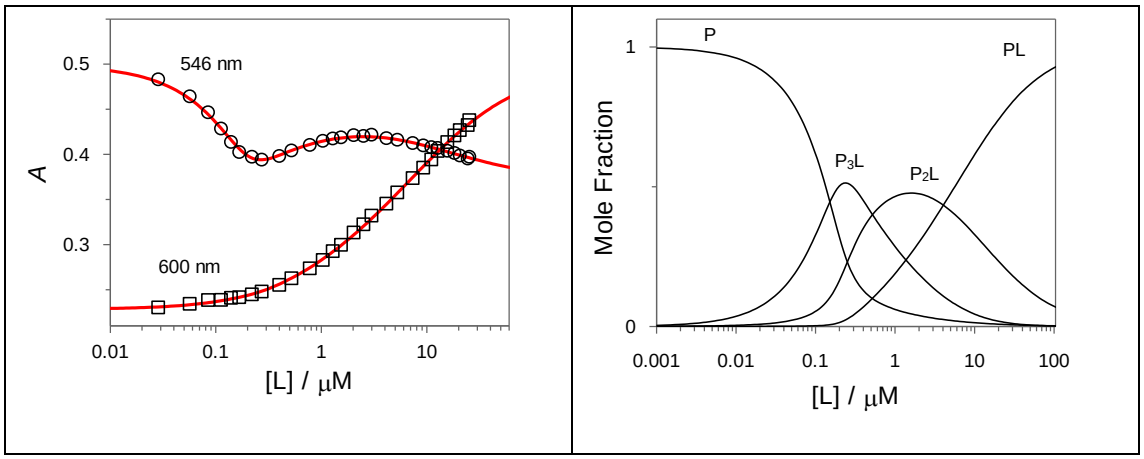

(A) **(B)**

Figure 3 - (A) Absorbance **P** (10 µM, pH = 1) at two different wavelengths as a function of **L** concentration. Global fitting was achieved with K_{11} = 3.7x10^5 M^{-1}, K_{12} = 2.1x10^6 M^{-1}, K_{13} = 6.8x10^5 M^{-1}, ε_{Lf}(546 nm) = 5.0x10^4 M^{-1}cm^{-1}, ε_{11}(546 nm) =3.7x10^4 M^{-1}cm^{-1}, ε_{12}(546 nm) =4.9x10^4 M^{-1}cm^{-1}, ε_{13}(546 nm) =3.0x10^4 M^{-1}cm^{-1}, ε_{Lf}(600 nm) = 2.3x10^4 M^{-1}cm^{-1}, ε_{11}(600 nm) =4.9x10^4 M^{-1}cm^{-1}, ε_{12}(600 nm) =2.2x10^4 M^{-1}cm^{-1}, ε_{13}(600 nm) =2.5x10^4 M^{-1}cm^{-1}; (B) Mole fraction distribution of the different **P** species as a function of **L** concentration.

Table 1 – Dye (**P** or **PD**)-lignin association constants (K_{a1}, K_a2 *and* K_{a3}) at pH 1.0 determined by UV-Visible spectroscopy. The error was estimated to be below 20%.

*Portisin (**P**)*			*Pyranoanthocyanin dímer (**PD**)*		
$\mathbf{K_{a1}}$ / $\mathbf{M^{-1}}$	$\mathbf{K_{a2}}$ / $\mathbf{M^{-1}}$	$\mathbf{K_{a3}}$ / $\mathbf{M^{-1}}$	$\mathbf{K_{a1}}$ / $\mathbf{M^{-1}}$	$\mathbf{K_{a2}}$ / $\mathbf{M^{-1}}$	$\mathbf{K_{a3}}$ / $\mathbf{M^{-1}}$
$3.7x10^5$	$2.1x10^6$	$6.8x10^5$	$1.6x10^4$	$3.1x10^6$	$1.7x10^6$

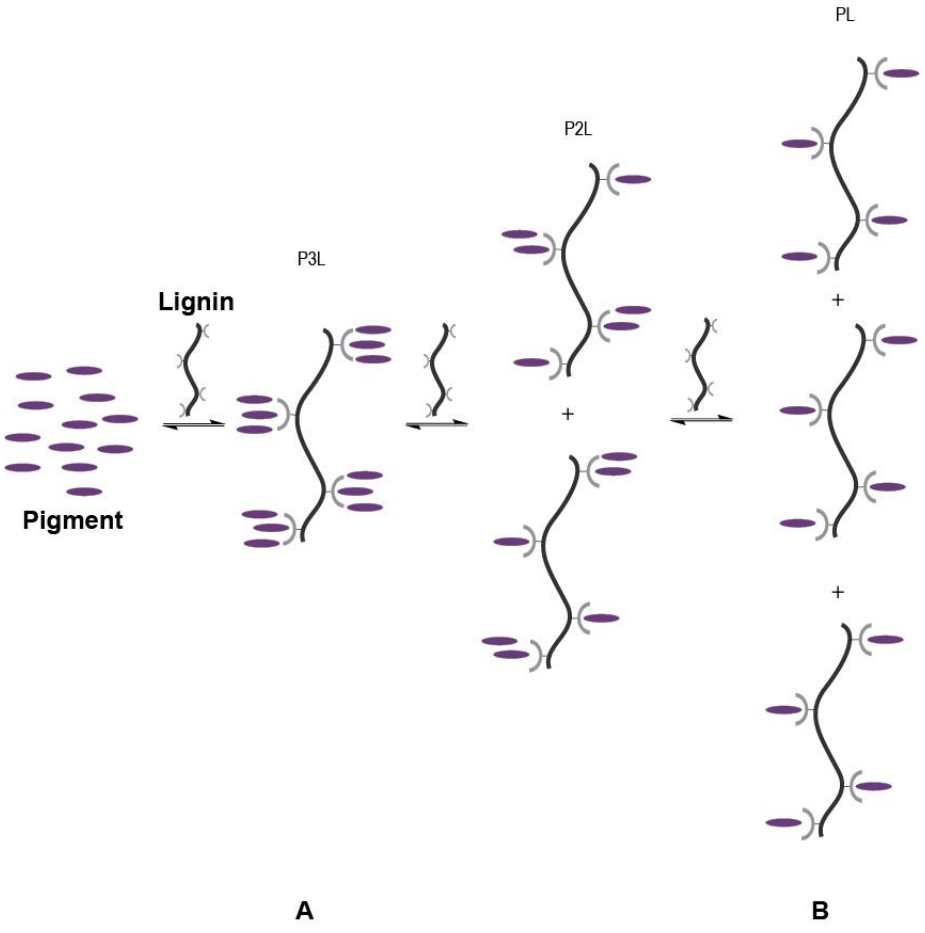

Figure 4 – Schematic representation of the interaction between the dye (**P** or **PD**) and lignin (**L**) with *n* binding sites. (A) for low concentrations of **L** (up to 0.27 µM), the aggregation of dyes is promoted by the lignin complexation (different molecules of the dye bind to the same site of lignin); (B) for higher concentrations of **L** (25 µM), the aggregation of dyes decreases (one molecule of dye bonded to each site of lignin) at pH 1.

3.2. Influence of lignin in the equilibrium forms of portisins and pyranoanthocyanin dimers at different pH values using UV-Visible spectroscopy.

Based on the strong interaction observed between **P** and **PD** with **L** at pH 1.0, the equilibrium forms of these dyes were studied in aqueous solutions at different pH values from 2.0 to 11.5 in the presence of a fixed concentration of **L** (19 μM) using UV-Visible spectroscopy and the results obtained are presented in **Figure 5** and **SI – Figure 3**.

The observation of **Figure 5a** shows that increasing the pH of the solutions from 2.0 to 7.3 yields to a decrease of the absorbance at ~ 570 nm and a displacement of the maximum absorption wavelength for lower values (hypsochromic shift). This is due to the equilibrium between the pyranoflavylium cation form and the neutral quinoidal form (**Figure 6**). When the pH increases from 7.3 up to 8.6 (**Figure 5b**), it is observed a small decrease of the absorbance at ~ 500 nm together with the appearance of a shoulder at ~ 630 nm, which is associated with the equilibrium between the neutral quinoidal base and the respective anionic base (**Figure 6**). For higher pH values (pH > 8.6) it is observed an increase of the absorbance at ~ 630 nm and a small bathochromic shift (**Figure 5c**) that is associated with the equilibrium between the anionic base and di-anionic base (**Figure 6**) as already reported in the literature for this dye without **L** [22].

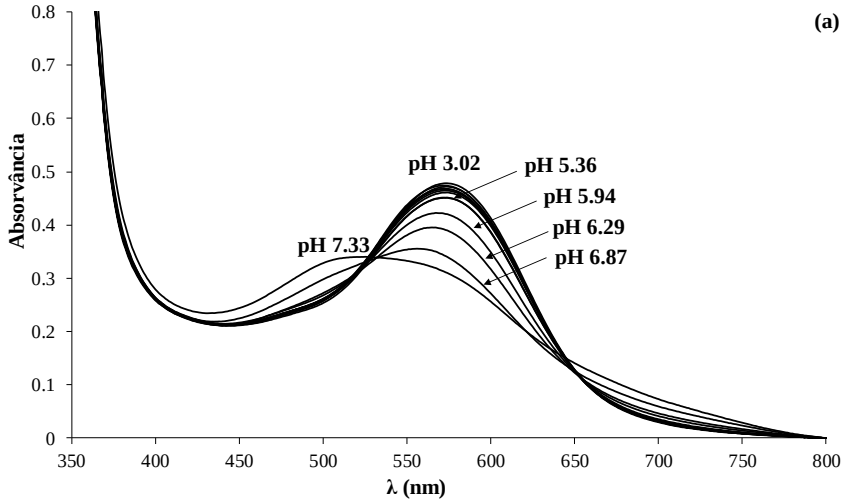

225

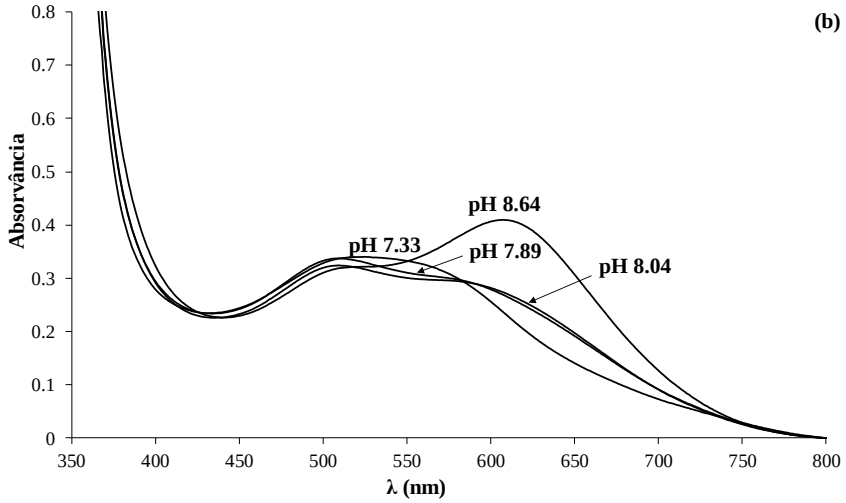

226

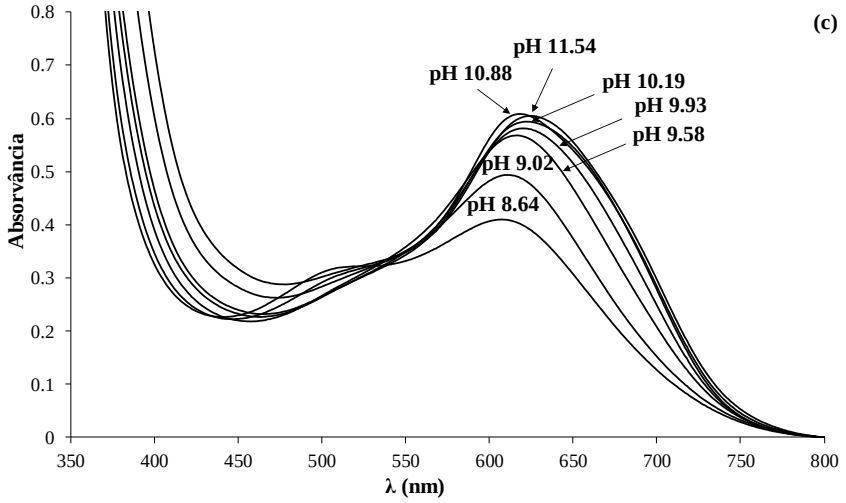

227

228 **Figure 5 –** Visible spectra (350 – 800 nm) of the solutions of **P** (44 μM) in the presence of **L** (19
229 μM) as a function of pH: (a), from pH 2.0 until 7.3; (b) from pH 7.3 up to 8.6 and (c) from pH 8.6
230 to 11.5.

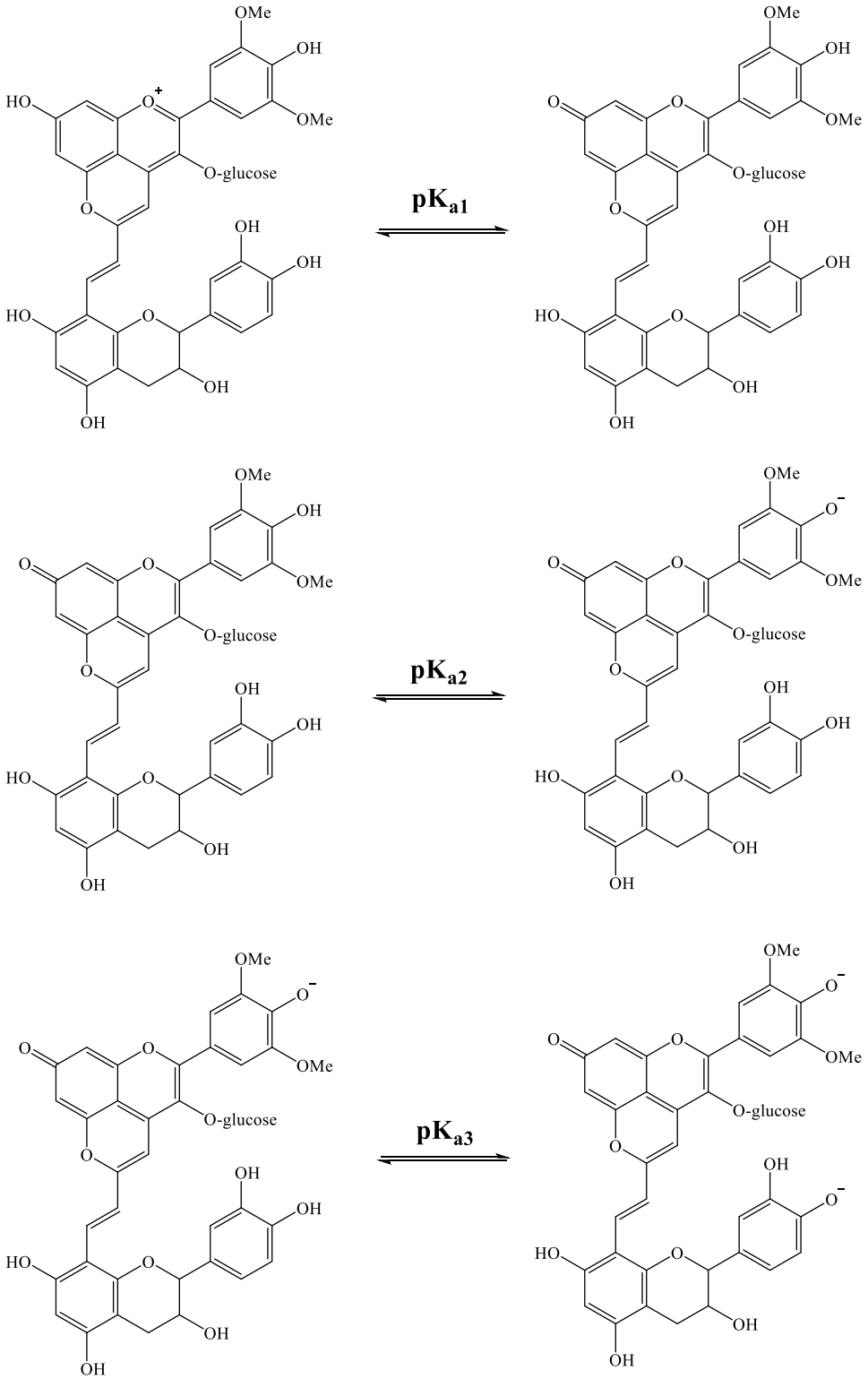

Figure 6 – Proton transfer equilibria of **P** in aqueous solutions at different pH values between 1 and 11.

Similarly, the same trend was also observed for **PD** in the presence of **L** as reported in **SI Figure 4**.

In addition, considering the four equilibrium species that are present in the pH range studied (2.0 to 11.5) and using the graphical representation of the absorbance at 500, 570 and 630 nm (in the case of **P**) as a function of the pH of the solution and their respective fitting (**Figure 7** and **SI – Figure 4**) it was possible to determine the three ionization constants ($pK^{\wedge}_{a1}$, $pK^{\wedge}_{a2}$ and $pK^{\wedge}_{a3}$) for **P and PD** in the presence of **L** (**Table 2**). The results obtained were compared with the ones reported in the literature for **P** and **PD** without **L** (**Table 2**) [22].

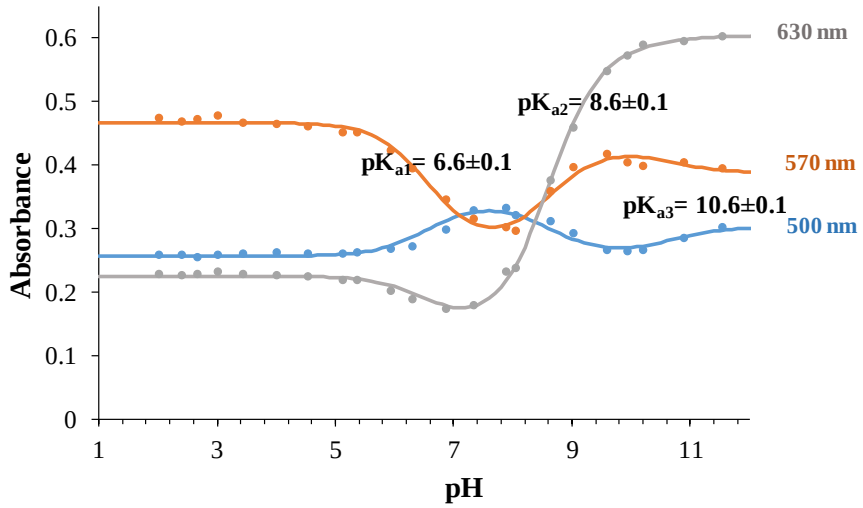

Figure 7 – Absorbance at 500, 570 and 630 nm as a function of the pH and respective fittings for the **P** (44 μM) in the presence of **L** (19 μM).

From **Table 2** it is possible to characterize the impact that **L** has on the stabilization of the pyranoflavylium cation forms of these two bluish dyes (**P** and **PD)** as the first ionization constants ($pK^{\wedge}_{a1}$) of **P** and **PD** in the presence of **L** are significantly higher ($pK^{\wedge}_{a1}$= 6.6±0.1 and $pK^{\wedge}_{a1}$= 6.2±0.1, respectively) than the ones observed for the same

253 dyes ($pK^{\wedge}_{a1}$= 4.61±0.03 and $pK^{\wedge}_{a1}$= 4.93±0.04, respectively) [22] without **L** at the
254 pseudo-equilibrium (**Figure 8** and **SI – Figure 5**).
255 Moreover, in the presence of **L** at equilibrium (**Table 2**) it was also possible to observe
256 the stabilization of the **P** and **PD** species, specially the pyranoflavylium cation forms
257 although in a smaller extent than at pseudo-equilibrium. With respect to pK_{a2} and pK_{a3},
258 the values obtained in the absence and presence of **L** were similar.
259 In fact, the presence of anionic sulfonate groups attached to the alkane backbone units of
260 lignin is thought to be at the origin of the strong stabilization of the pyranoflavylium
261 cation form of the dyes.
262
263 **Table 2 –** Ionization constants of **P** and **PD** at pseudo-equilibrium ($pK^{\wedge}_{a}$) and equilibrium ($pK^{\prime}_{a}$) in
264 the absence [22] and presence of **L**, determined by UV-VIS spectroscopy.

	without L [22]			**with lignin (19 µM)**					
	at pseudo-equilibrium			at pseudo-equilibrium			at equilibrium		
	$pK^{\wedge}_{a1}$	**$pK^{\wedge}_{a2}$**	**$pK^{\wedge}_{a3}$**	**$pK^{\wedge}_{a1}$**	**$pK^{\wedge}_{a2}$**	**$pK^{\wedge}_{a3}$**	**$pK^{\prime}_{a1}$**	**$pK^{\prime}_{a2}$**	**$pK^{\prime}_{a3}$**
P	4.61±0.03	8.36±0.03	10.11±0.06	6.6±0.1	8.6±0.1	10.6±0.1	6.38±0.1	7.76±0.1	10.5±0.1
PD	4.93±0.04	8.33±0.04	9.1±0.04	6.2±0.1	9.5±0.1	9.9±0.1	5.90±0.1	7.74±0.1	8.86±0.1

265

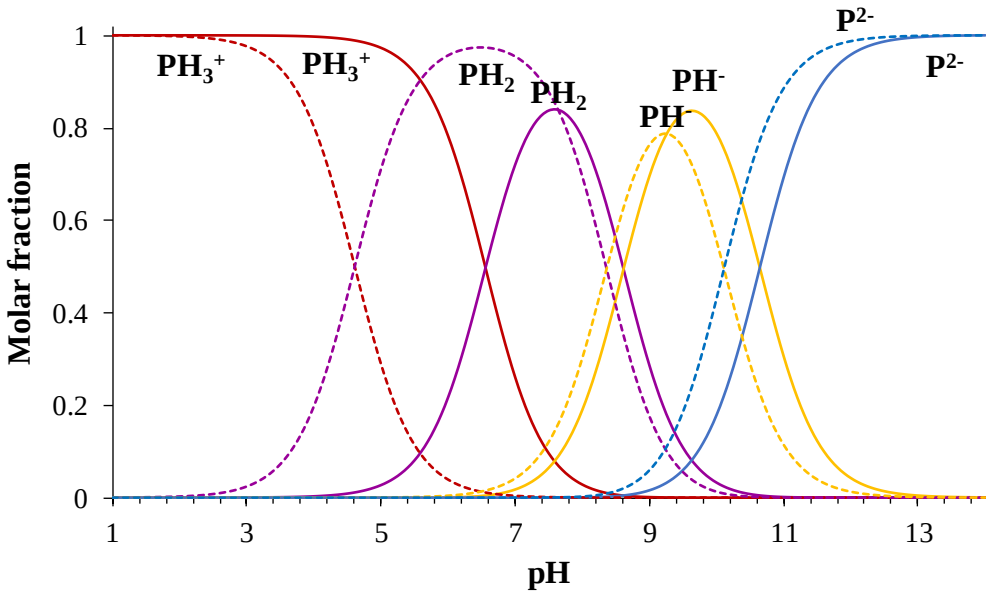

Figure 8 – Molar fraction distribution diagram for **P** in the absence (dashed lines) and presence (solid lines) of **L** as a function of pH determined by UV-Visible spectroscopy.

3.3. Impact of lignin on the solubility and stability of the dyes.

According to the results obtained so far, it seems that calcium lignosulfonate strongly interacts with portisins and pyranoanthocyanin dimers stabilizing their pyranoflavylium cation form. Moreover, knowing that this sulfonated lignin derivative is highly soluble in water and that the blue dyes (**P** and **PD**) need to improve their solubility in aqueous systems it was evaluated the impact of **L** on the solubility of the dyes at different concentration over time, using turbidimetry.

For that, solutions containing different concentrations of dye (20, 40, 80 and 160 μM) were prepared in citrate buffer at pH 3.5 in the absence and in the presence of **L** (19 μM) and the solutions were left at room temperature in the dark during 30 days. To evaluate the stability of dyes with and without **L**, spectra of the solutions were recorded at different points 0, 1, 3, 6 and 30 days and the results are presented in **Figure 9** for the lower

concentration (20 μM) of **P**. On the other hand, the turbidity of all the solutions were measured initially, after one day and after 30 days (**Table 3**).

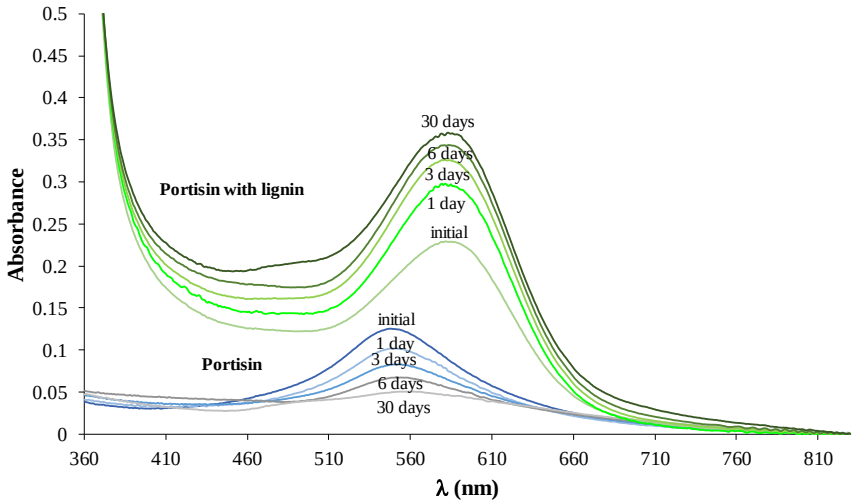

Figure 9 – Absorption spectra of **P** (20 μM) in the absence and presence of **L** (19 μM) at the day 0, 1, 3, 6 and 30.

From **Figure 9** it is possible to observe that in the absence of **L**, the colour of **P** fades with time, as the initial absorbance at the maximum absorption wavelength (~560 nm) decreases after one, three, six and thirty days. Moreover, as referred before the addition of **L** yields to an important increase on the absorption of dyes along with a significant bathochromic shift in the maximum absorption wavelength (~40 nm). This colour intensification increases with time being more pronounced after thirty days when compared to the initial solution. A similar behaviour was also observed for the other dye concentration 40, 80 and 160 μM and for **PD** (**SI – Figure 6**).

Concerning the solubility of the dyes that were evaluated by turbidimetry, it seems that the dyes turbidity increases along with the concentration (**Table 3**). In the absence of **L**, the turbidity of the solution remains constant over time regardless of the dyes concentration. On the other hand, when **L** is added the turbidity of the solutions is not greatly affected (day 0) being higher in this case for the **PD**. However, over time the

turbidity of the solutions containing **L** seems to decrease comparatively with the ones without **L** (**Table 3**).

After thirty days, it is possible to observe that the solutions containing the dyes alone (**P** and **PD)** loose some of their colour due to the low solubility of the compounds in aqueous systems over time and eventually precipitate (**Figure 10**). However, when the solutions containing **P+L** and **PD+L** after thirty days are compared with the starting point (day 0) it is observed an intensification of the colour for all concentrations of dye tested (**Figures 9 and 10**).

Table 3 – Turbidity (NTU) of solutions of **P** and **PD** at different concentrations (20, 40, 80 and 160 μM) in the absence and presence of **L** (19 μM).

			Day 0	**Day 1**	**Day 30**
	|Dye| (μM)	**|Lignin| (μM)**	**Turbidity (NTU) ± SD**	**Turbidity (NTU) ± SD**	**Turbidity (NTU) ± SD**
P	20	0	11.4±0.1	9.4±0.4	8.6±0.4
	40		23.1±0.5	22±1	21±1
	80		45±1	46.1±0.7	40±1
	160		98±2	101±2	87.1±0.6
	20	19	18.6±0.2	13.8±0.1	8.2±0.1
	40		28.5±0.5	18.8±0.5	12.7±0.2
	80		44.1±0.4	26±1	22.5±0.2
	160		82±1	47.9±0.6	29.8±0.2
PD	20	0	9.3±0.2	9.5±0.6	8.5±0.4
	40		18.8±0.1	19.2±0.1	20.3±0.6
	80		38.5±0.4	38±1	39±1
	160		72.4±0.8	74±2	70±7
	20	19	19.7±0.7	16.8±0.6	10.7±0.1
	40		29.8±0.3	23.9±0.4	12.9±0.5
	80		50±2	39±1	13.6±0.2
	160		93±2	70±1	26.9±0.3

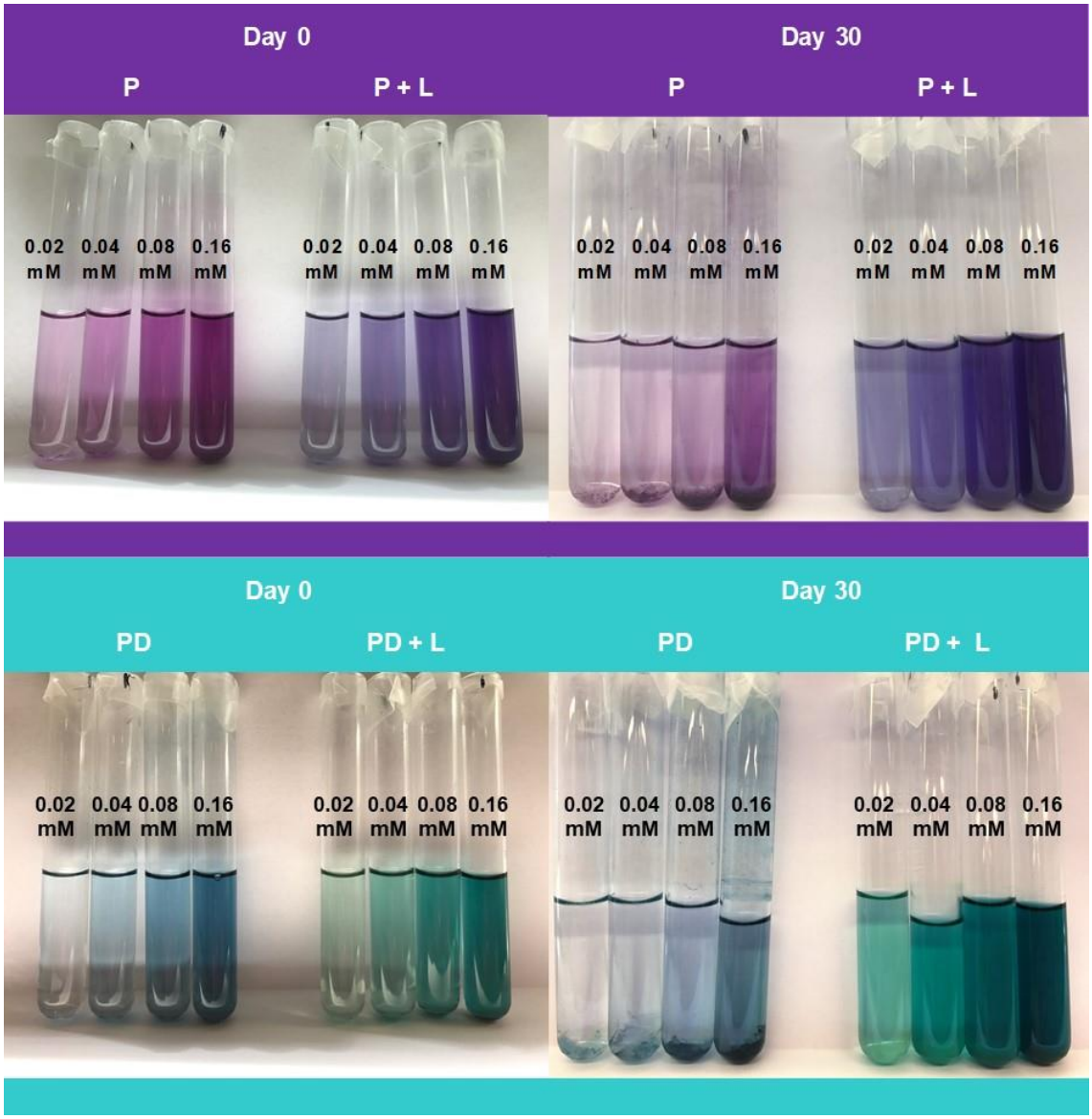

Figure 10 – Colour of the solutions of **P** and **PD** at different concentrations (20, 40, 80 and 160 μM) in the absence and presence of **L** (19 μM) in citrate buffer pH 3.5 at day 0 and after 30 days in the dark.

Overall, the results obtained from the interaction of a lignosulfonate with bluish anthocyanin-derived dyes (portisins and pyranoanthocyanin dimers) and its impact on the chromatic features of these pigments showed an important stabilization of the pyranoflavylium form of the dyes. Thus, this macromolecule can be used as a tool to stabilize and modulate the colour of natural bluish dyes and to improve their solubility in aqueous systems.

4. Literature cited

[1] Mateus N, Silva AMS, Rivas-Gonzalo JC, Santos-Buelga C, De Freitas V. A new class of blue anthocyanin-derived pigments isolated from red wines. J Agric Food Chem. 2003;51(7):1919-23.

[2] Oliveira J, Azevedo J, Silva AMS, Teixeira N, Cruz L, Mateus N, de Freitas V. Pyranoanthocyanin dimers: a new family of turquoise blue anthocyanin-derived pigments found in Port wine. J Agric Food Chem. 2010;58(8):5154-9.

[3] Hatakeyama H, Hatakeyama T. Lignin Structure, Properties, and Applications. In: Abe A, Dusek K, Kobayashi S, editors. Biopolymers: Springer Berlin Heidelberg; 2010. p. 1-63.

[4] Stewart D. Lignin as a base material for materials applications: Chemistry, application and economics. Industrial Crops and Products. 2008;27(2):202-7.

[5] Saito T, Brown RH, Hunt MA, Pickel DL, Pickel JM, Messman JM, Baker FS, Keller M, Naskar AK. Turning renewable resources into value-added polymer: development of lignin-based thermoplastic. Green Chemistry. 2012;14(12):3295-303.

[6] Mendu V, Shearin T, Campbell JE, Stork J, Jae J, Crocker M, Huber G, DeBolt S. Global bioenergy potential from high-lignin agricultural residue. Proceedings of the National Academy of Sciences. 2012;109(10):4014-9.

[7] Aro T, Fatehi P. Production and Application of Lignosulfonates and Sulfonated Lignin. ChemSusChem. 2017;10(9):1861-77.

[8] SenGupta A, Spindler R, Darlington J. Multifunctional particulate additive for personal care and cosmetic compositions, and the process of making the same. Google Patents; 2003.

348 [9] Murphy RT. Cosmetic deodorant compositions containing encapsulated bicarbonate
349 and liquid fragrance ingredients. Google Patents; 1996.
350 [10] Küster FW, Thiel A. Tabelle per le Analisi Chimiche e Chimico- Fisiche. 12 th ed.
351 Milano, Italy: Hoepli; 1982. p. 157-60.
352 [11] Mateus N, Oliveira J, Santos-Buelga C, Silva AMS, de Freitas V. NMR structure
353 characterization of a new vinylpyranoanthocyanin-catechin pigment (a portisin).
354 Tetrahedron Lett. 2004;45(17):3455-7.
355 [12] Leydet Y, Gavara R, Petrov V, Diniz AM, Jorge Parola A, Lima JC, Pina F. The
356 effect of self-aggregation on the determination of the kinetic and thermodynamic
357 constants of the network of chemical reactions in 3-glucoside anthocyanins.
358 Phytochemistry. 2012;83(0):125-35.
359 [13] Kim O-K, Je J, Jernigan G, Buckley L, Whitten D. Super-Helix Formation Induced
360 by Cyanine J-Aggregates onto Random-Coil Carboxymethyl Amylose as Template. J Am
361 Chem Soc. 2006;128(2):510-6.
362 [14] Gadde S, Batchelor EK, Kaifer AE. Controlling the Formation of Cyanine Dye H-
363 and J-Aggregates with Cucurbituril Hosts in the Presence of Anionic Polyelectrolytes.
364 Chemistry – A European Journal. 2009;15(24):6025-31.
365 [15] Moreno-Villoslada I, Fuenzalida JP, Tripailaf G, Araya-Hermosilla R, Pizarro GdC,
366 Marambio OG, Nishide H. Comparative Study of the Self-Aggregation of Rhodamine 6G
367 in the Presence of Poly(sodium 4-styrenesulfonate), Poly(N-phenylmaleimide-co-acrylic
368 acid), Poly(styrene-alt-maleic acid), and Poly(sodium acrylate). The Journal of Physical
369 Chemistry B. 2010;114(37):11983-92.
370 [16] Moreno-Villoslada I, Torres-Gallegos C, Araya-Hermosilla R, Nishide H. Influence
371 of the Linear Aromatic Density on Methylene Blue Aggregation around Polyanions

372 Containing Sulfonate Groups. The Journal of Physical Chemistry B. 2010;114(12):4151-
373 8.
374 [17] Kozlova NO, Bruskovskaya IB, Okuneva IB, Melik-Nubarov NS, Yaroslavov AA,
375 Kabanov VA, Menger FM. Interaction of a cationic polymer with negatively charged
376 proteoliposomes. Biochimica et Biophysica Acta (BBA) - Biomembranes.
377 2001;1514(1):139-51.
378 [18] Basílio N, Piñeiro Á, Da Silva JP, García-Río L. Cooperative Assembly of Discrete
379 Stacked Aggregates Driven by Supramolecular Host–Guest Complexation. The Journal
380 of Organic Chemistry. 2013;78(18):9113-9.
381 [19] Trouillas P, Sancho-García JC, De Freitas V, Gierschner J, Otyepka M, Dangles O.
382 Stabilizing and modulating color by copigmentation: insights from theory and
383 experiment. Chemical Reviews. 2016;116(9):4937-82.
384 [20] Le VH, Buscaglia R, Chaires JB, Lewis EA. Modeling complex equilibria in
385 isothermal titration calorimetry experiments: Thermodynamic parameters estimation for
386 a three-binding-site model. Anal Biochem. 2013;434(2):233-41.
387 [21] Vega S, Abian O, Velazquez-Campoy A. A unified framework based on the binding
388 polynomial for characterizing biological systems by isothermal titration calorimetry.
389 Methods. 2015;76(Supplement C):99-115.
390 [22] Oliveira J, Mateus N, de Freitas V. Previous and recent advances in
391 pyranoanthocyanins equilibria in aqueous solution. Dyes and Pigments. 2014;100(0):190-
392 200.

393

394 **ACKNOWLEDGEMENTS**

395 This work received financial support from FEDER funds through COMPETE,
396 POPH/FSE, QREN and FCT (Fundação para a Ciência e Tecnologia) by two post-

doctoral scholarships (SFRH/BPD/112465/2015, SFRH/BPD/84805/2012), an investigator contract (IF/00225/2015) and grants PTDC/AGR-TEC/2789/2014 COMPETE POCI-01-0145-FEDER-016616, REDE/1517/RMN/2005. This work also received financial support (UID/QUI/50006/2013 - POCI/01/0145/FEDER/007265) from FCT/MEC through national funds and co-financed by FEDER, under the Partnership Agreement PT2020 and FEDER-Interreg España-Portugal Programme (Project ref. 0377_IBERPHENOL_6_E).

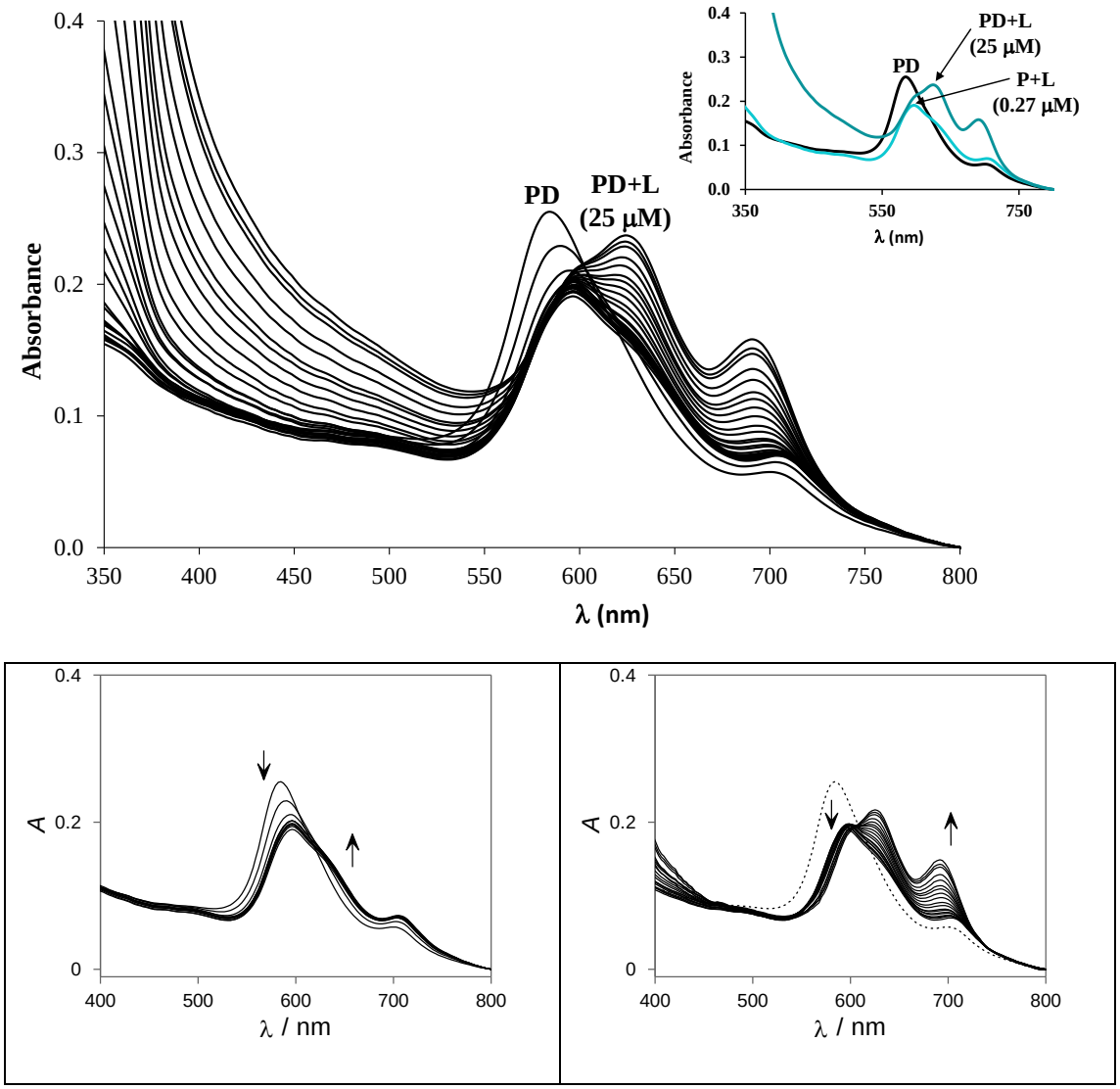

Figure 11 – Visible spectra of **PD** with different concentrations of **L** and the inset shows the spectrum of the pigment in the absence and in the presence of the maximum concentration of **L** (0.025 mM) at pH 1. Visible spectra of **PD** ($1x10^{-5}$ M) at pH = 1 with different concentrations of **L**. (left) From 0 to $4.0x10^{-7}$ M and (right) from $4.0x10^{-7}$ M to $2.77x10^{-5}$ M of **L**. The spectrum of **PD** in the absence of **L** is also shown for comparison (dotted line). All spectra were corrected by subtracting the corresponding absorption of **L**.

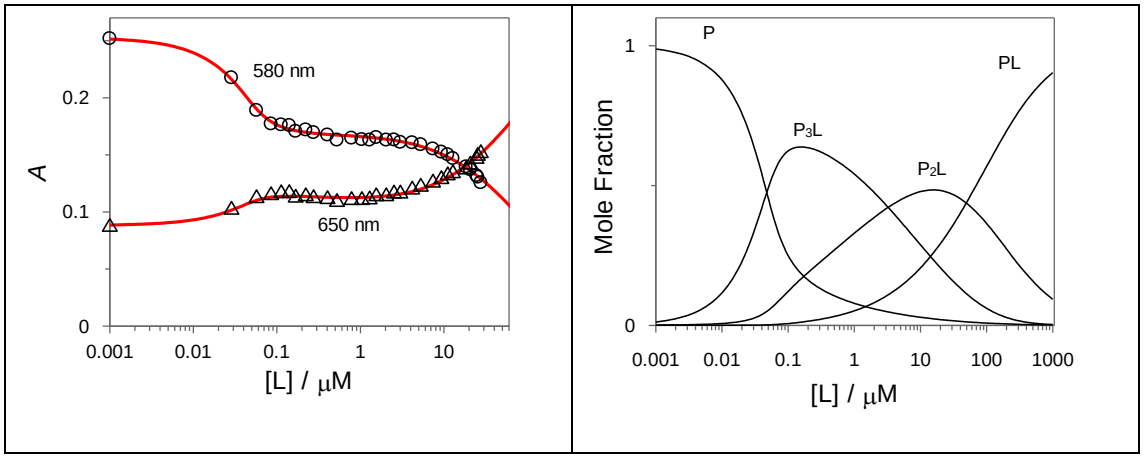

Figure 2 - (a) Absorbance **PD** (10 μM, pH = 1) at two different wavelengths as a function of lignin **L** concentration; (b) Mole fraction distribution of the different **PD** species ad a function of **L** concentration.

406

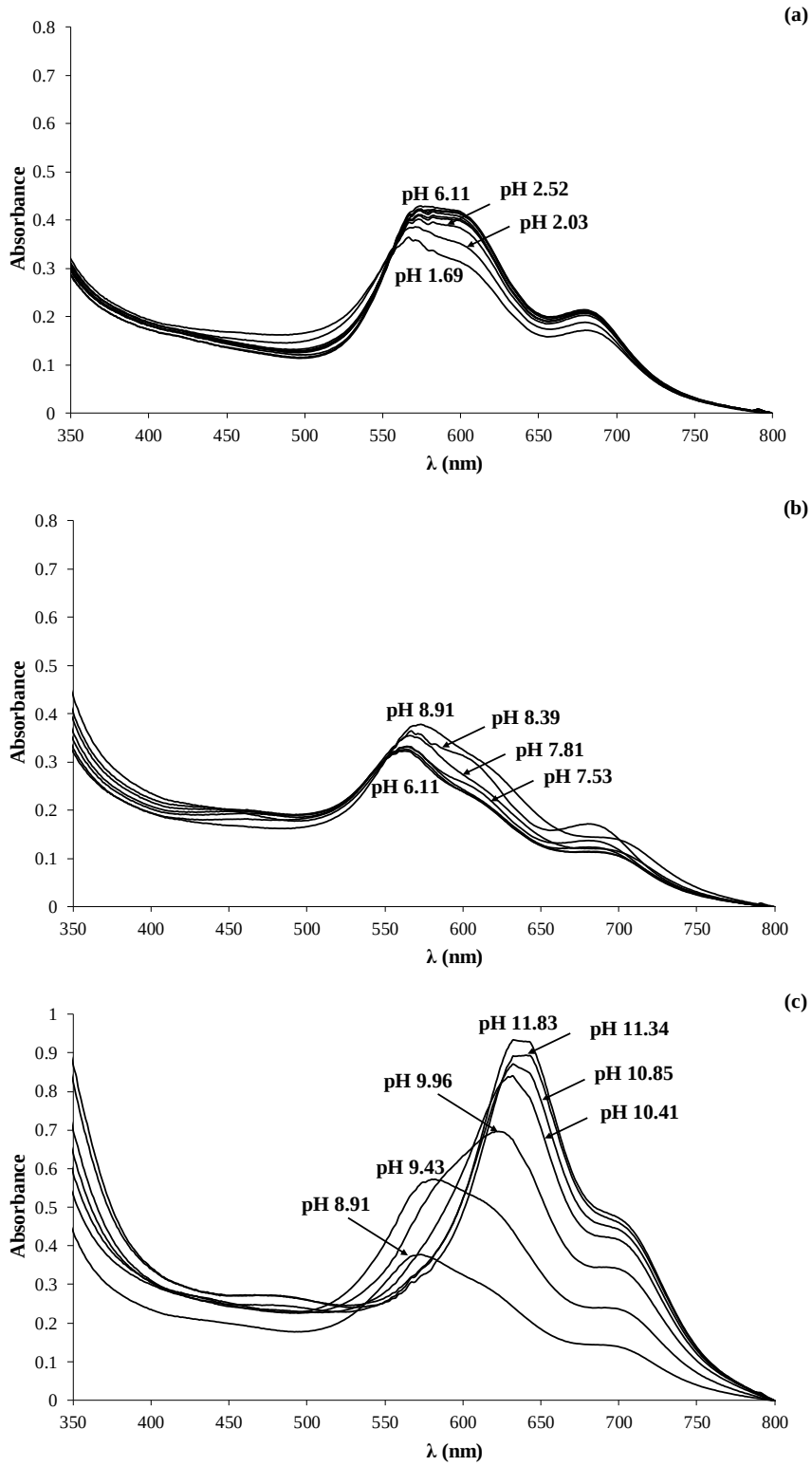

Figure 3 - Visible spectra (350 – 800 nm) of the solutions of PD (44 µM) in the presence of L (19 µM) as a function of pH: (a), from pH 1.7 until 6.1; (b) from pH 6.1 up to 8.9 and (c) from pH 8.9 to 11.8.

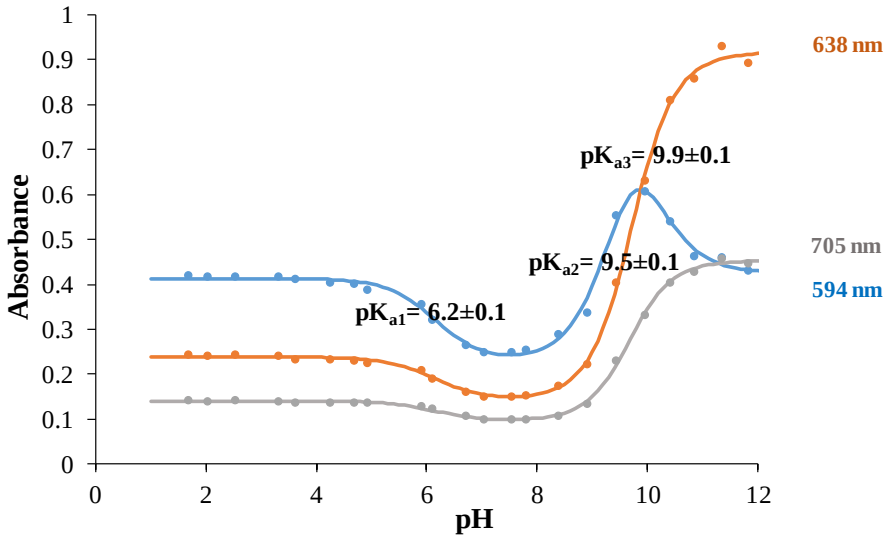

Figure 4 – Absorbance at 594, 638 and 705 nm as a function of the pH and respective fittings for the PD (44 µM) in the presence of L (19 µM).

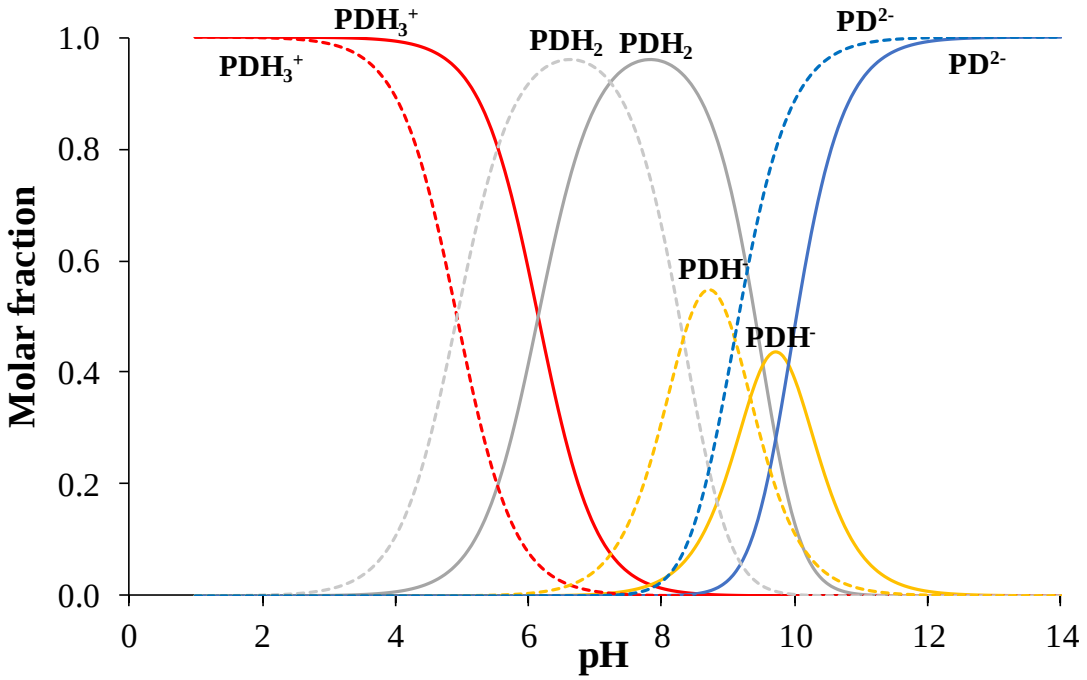

Figure 5 – Molar fraction distribution diagram for PD in the absence (dashed lines) and presence (solid lines) of L as a function of pH determined by UV-Visible spectroscopy.

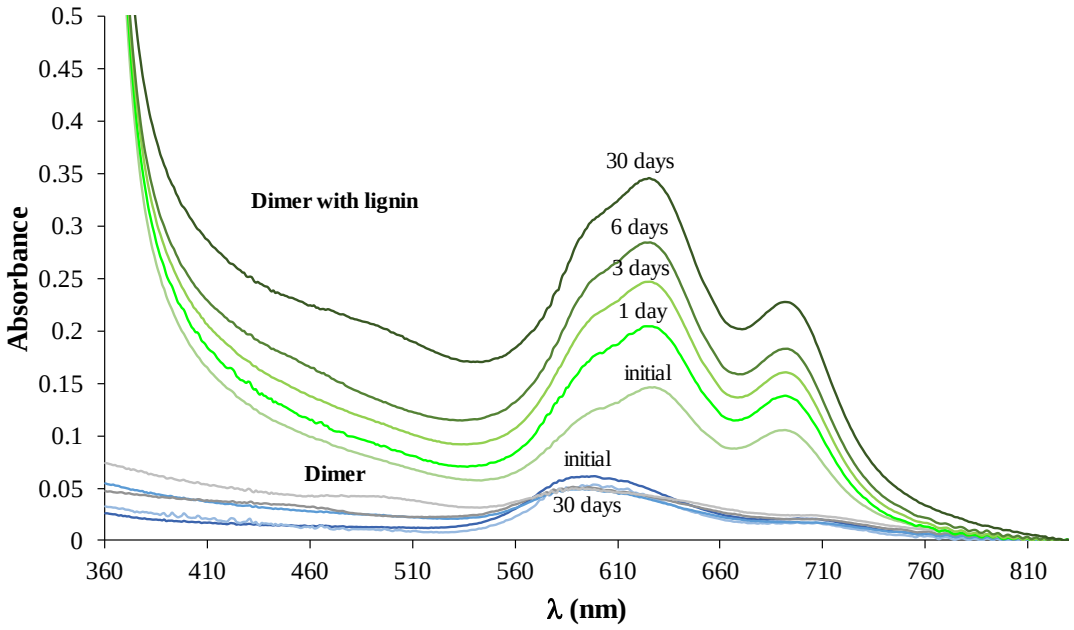

Figure 6 – Absorption spectra of PD (20 μM) in the absence and presence of L (19 μM) at the day 0, 1, 3, 6 and 30.